Efficient Analysis of Quasi-Optical Filters by a Hybrid MoM/BI-RME Method

Maurizio Bozzi, *Member, IEEE*, Luca Perregrini, *Member, IEEE*, Jochen Weinzierl, and Carsten Winnewisser

***Abstract*—This paper presents a novel algorithm for the analysis of quasi-optical filters, consisting of thick metal screens perforated periodically with arbitrarily shaped apertures. The algorithm is based on the widely used method of moments (MoM) in conjunction with entire domain basis functions. Its flexibility, accuracy, and rapidity depend on the use of the Boundary Integral-Resonant Mode Expansion (BI-RME) method in the numerical determination of the basis functions. A computer code has been developed based on this algorithm. The analysis of two different quasi-optical filters operating at 8 GHz and 280 GHz is reported and compared with experimental data as well as with other simulations. In both cases, the whole analysis requires few seconds on a standard workstation and the theoretical results show a very good agreement with the measured data in a wide frequency band. The capability of the MoM/BI-RME approach to handle completely arbitrary shapes is highlighted in the second example. In this case, in fact, the fabrication process causes small deformations of the nominal shape of the apertures, which must be accounted for, since they play an important role in the frequency response of the filter.**

***Index Terms*—Coupling integrals, entire domain basis functions, frequency-selective surfaces, numerical methods, quasi-optical filters.**

I. Introduction

QUASI-OPTICAL filters typically consist of a metal screen perforated periodically with apertures (Fig. 1) and find several applications in the microwave as well as in the millimeter– and submillimeter-wave range [1]–[3]. The reflection/transmission characteristics of the filters depend on the shape of the apertures, on their size and spacing, and on the thickness of the metal screen.

Many different algorithms have been proposed for the analysis of quasi-optical filters under the infinite array approximation: the method of moments (MoM) [4], [5], the finite difference time-domain (FDTD) method [6], and the finite element method (FEM) [7]. Algorithms based on the FDTD or FEM apply to very general structures but are usually quite slow and require large memory allocation. This problem can be partially overcome by using hybrid methods [8]–[12]. The MoM is a widely used method and has been applied with both subdomain [4] and entire domain basis functions [5] to expand the fields on the apertures. Subdomain basis functions apply to arbitrary apertures, but lead to large matrix problems and are limited to thin screens. Conversely, the use of entire domain basis functions reduces the dimension of the matrix problem, thus leading to a very efficient algorithm. The modal vectors of a waveguide with a cross section coincident with the aperture represent a suitable set of basis functions, since they span the entire domain of the aperture and satisfy the boundary conditions [13], [14]. This choice, indeed, is quite obvious in the case of thick screens, since each hole perforating the screen can be considered as a short waveguide section. In [5], analysis is limited to structures with apertures of conventional shape (e.g., rectangular or circular), where the modal vectors are known analytically. On the other hand, different shapes, such as crosses [15], [16], Jerusalem crosses [4], [16], tripoles [17], [18], rings, and square loops [19], [20], are useful for obtaining better performances (e.g., stability of the resonance frequency with the incident angle, low cross-polarization level, large bandwidth, small band separation). Moreover, considering irregular shapes is important in high accuracy analyses, to take into account small deformations of the apertures due to the manufacturing process. Therefore, a CAD tool for the analysis of quasi-optical filters should be able to consider arbitrarily shaped apertures. In this case, the modal vectors of the waveguide must be numerically calculated.

In this paper, we present the application of the MoM in conjunction with the Boundary Integral-Resonant Mode Expansion (BI-RME) method [21]–[23], which is used in the numerical calculation of the waveguide modes. The BI-RME method applies to arbitrary apertures and permits one to calculate the set of entire domain basis functions in a very short time. Moreover, it

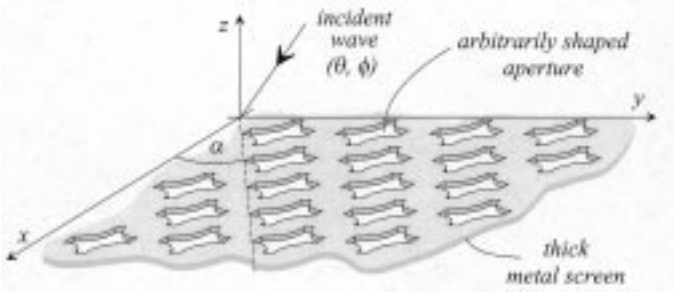

Fig. 1. A quasi-optical filter with arbitrarily shaped apertures.

Manuscript received August 8, 1999; revised December 18, 2000. This work was supported by the European Commission under the TMR Research Programme Contract N. ERBFMRXCT960050, by the University of Pavia under F.A.R. Funding, and by the Deutsche Forschungsgemeinschaft (DFG) through Sonderforschungsbereich 276.

M. Bozzi and L. Perregrini are with the Department of Electronics of the University of Pavia, 27100 Pavia, Italy (e-mail: m.bozzi@ele.unipv.it; l.perregrini@ele.unipv.it).

J. Weinzierl is with the University of Erlangen-Nürnberg, 91058 Erlangen, Germany (e-mail: jochen@lhft.e-technik.uni-erlangen.de).

C. Winnewisser was with Department of Molecular and Optical Physics of the University of Freiburg, 79104 Freiburg, Germany. He is now with the R&D Pump Laser Group of JDS Uniphase, CH-8045 Zürich, Switzerland (e-mail: carsten.winnewisser@ch.jdsuniphase.com).

Publisher Item Identifier S 0018-926X(01)05647-2.

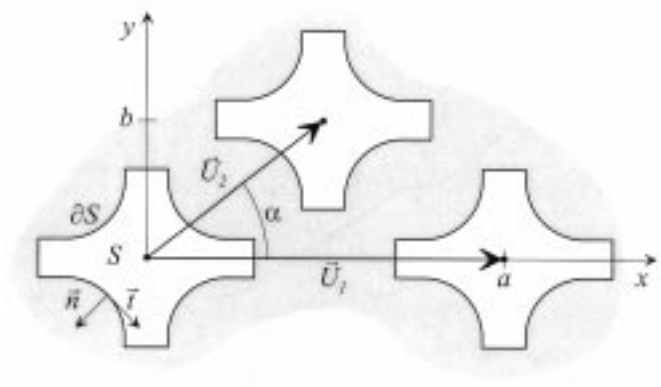

Fig. 2. Periodicity of the quasi-optical structure: $\vec{U}_1 = a\vec{u}_x$, $\vec{U}_2 = b/\tan\alpha\vec{u}_x + b\vec{u}_y$.

will be shown that this method yields as a by-product quantities involved in the calculation of the MoM matrices.

In order to demonstrate the capabilities of the proposed method, we present the analysis of two quasi-optical filters. The first example refers to a very thick X-band dichroic filter, excited by a plane wave at an oblique angle of incidence. In this case, we can obtain very good results, both compared with experimental data and with theoretical results calculated by using a different numerical method. The second example is a bandpass filter at 280 GHz consisting of a metal screen perforated with cross-shaped apertures, excited by a plane wave with normal incidence. By exploiting the capability of the code in handling arbitrarily shaped apertures, we can take into account the effect of the rounded corners due to the manufacturing process. The comparison between numerical and experimental results over a very wide frequency band demonstrates the accuracy of the method and highlights the possibility of dramatically shortening the computing time with respect to commercially available codes.

II. MoM Analysis of Quasi-Optical Filters

The MoM analysis of quasi-optical filters is a well-established technique [1]. The only aim of this short overview is the introduction of formulas and symbols relevant for the discussion to follow.

Let us consider a quasi-optical filter (Fig. 1) consisting of a thick metal screen, perforated periodically with apertures of arbitrary shape. The aim of the analysis is the determination of the reflected and transmitted electromagnetic fields when the filter is illuminated by a uniform plane wave at a given angular frequency ω, incident from the direction (θ, ϕ).

Due to the double periodicity of the structure (Fig. 2), the analysis reduces to the investigation of a single unit cell [1]. By using the equivalence theorem, apertures S_1 and S_2 on both sides of the screen (see Fig. 3) are closed by perfect conductors, and equivalent magnetic current densities $\vec{M}_1$ and $\vec{M}_2$ are defined over them. In order to guarantee the continuity of the tangential component of the electric field, we impose that the magnetic currents on both sides of S_1 and S_2 are equal in amplitude and opposite in phase. Moreover, to ensure the continuity

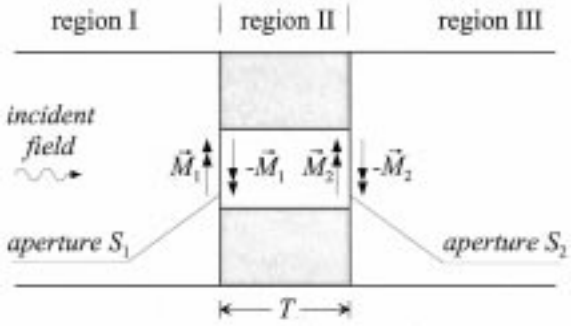

Fig. 3. Side view of the equivalent circuit of the unit cell. Region II is a waveguide section with a cross section S, connected to Regions I and III through the apertures S_1 and S_2, respectively.

of the tangential component of the magnetic field, the following equations must be satisfied:

$$\begin{cases} \left(2\vec{H}^{L_1}_{\text{inc}} + \vec{H}^{L_1}_{M_1}\right) \times \vec{u}_z = \left(\vec{H}^{R_1}_{M_1} + \vec{H}^{R_1}_{M_2}\right) \times \vec{u}_z & \text{on } S_1 \\ \left(\vec{H}^{L_2}_{M_1} + \vec{H}^{L_2}_{M_2}\right) \times \vec{u}_z = \vec{H}^{R_2}_{M_2} \times \vec{u}_z & \text{on } S_2 \end{cases} \tag{1}$$

where $\vec{H}_{\text{inc}}$ is the incident magnetic field, the subscripts refer to the source generating the field (namely, the incident field, $\vec{M}_1$, or $\vec{M}_2$), and the superscripts indicate the left and right sides of the pertinent aperture. The magnetic fields $\vec{H}^{L_1}_{M_1}$ and $\vec{H}^{R_2}_{M_2}$ (in region I and III, respectively) are expressed as summations of Floquet modes $\vec{\mathcal{H}}_{mn}$ (see Table I), whereas in region II the fields $\vec{H}^{R_1}_{M_1}$, $\vec{H}^{R_1}_{M_2}$, $\vec{H}^{L_2}_{M_1}$, and $\vec{H}^{L_2}_{M_2}$ are given as summations of magnetic modal vectors $\vec{h}_r$ of the waveguide with a cross section S (see Fig. 2).

As is well known, the magnetic modal vectors $\vec{h}_r$ of a waveguide can refer to both TM and TE modes. In the following, when necessary, prime and double prime superscripts will be used to distinguish between TM and TE modes, respectively. The magnetic modal vectors can be expressed in terms of two potential functions

$$\vec{h}'_r = -\vec{u}_z \times \frac{1}{\kappa'_r}\nabla_T\psi_r \tag{2}$$

$$\vec{h}''_r = -\frac{1}{\kappa''_r}\nabla_T\phi_r \tag{3}$$

where κ'_r and κ''_r are the cutoff wavenumber of the TM and TE modes, respectively. The potentials ψ_r and ϕ_r satisfy the Helmholtz equation with the Dirichelet and Neumann boundary conditions, respectively

$$\begin{cases} \nabla^2_T\psi_r + \kappa'^2_r\psi_r = 0 & \text{in S} \\ \psi_r = 0 & \text{on } \partial S \end{cases} \tag{4}$$

$$\begin{cases} \nabla^2_T\phi_r + \kappa''^2_r\phi_r = 0 & \text{in } S \\ \partial\phi_r/\partial n = 0 & \text{on } \partial S \end{cases} \tag{5}$$

Moreover, we assume the following normalization for the modal vectors:

$$\int_S \vec{h}_r \cdot \vec{h}_q \, dS = \delta_{rq} \tag{6}$$

TABLE I
EXPRESSIONS OF THE FLOQUET MODES ($k_0 = \omega\sqrt{\epsilon_0\mu_0}$; $\eta_0 = \sqrt{\mu_0/\epsilon_0}$; ϵ_0 AND μ_0 ARE THE ELECTRIC AND MAGNETIC PERMITTIVITIES OF THE VACUUM; $\nabla_T = \vec{u}_x\partial/\partial x + \vec{u}_y\partial/\partial y$)

	TM	TE	TEM (*)
Helmholtz equation	$\nabla_T^2\chi_{mn} + k_{mn}^2\chi_{mn} = 0$		$\nabla_T^2\chi_{10}^0 = \nabla_T^2\chi_{01}^0 = 0$
Cutoff wavenumber	$k_{x_{mn}} = k_0\sin\theta\cos\phi + \frac{2\pi m}{a}$ $k_{y_{mn}} = k_0\sin\theta\sin\phi + \frac{2\pi n}{b} - \frac{2\pi m}{a\tan\alpha}$ $k_{mn} = \sqrt{k_{x_{mn}}^2 + k_{y_{mn}}^2}$ $(m,n = 0,\pm1,\ldots)$		$k_{10}^0 = k_{01}^0 = 0$
Potential	$\chi_{mn} = -\frac{j}{\sqrt{ab}}e^{-j(k_{x_{mn}}x + k_{y_{mn}}y)}$		$\chi_{10}^0 = -\frac{x}{\sqrt{ab}}$ $\chi_{01}^0 = -\frac{y}{\sqrt{ab}}$
Magnetic modal field	$\vec{\mathcal{H}}'_{mn} = -\vec{u}_z \times \frac{\nabla_T\chi_{mn}}{k_{mn}}$	$\vec{\mathcal{H}}''_{mn} = -\frac{\nabla_T\chi_{mn}}{k_{mn}}$	$\vec{\mathcal{H}}_{10}^0 = -\vec{u}_z \times \nabla_T\chi_{10}^0$ $\vec{\mathcal{H}}_{01}^0 = -\vec{u}_z \times \nabla_T\chi_{01}^0$
Propagation constant	$\Gamma_{mn} = \begin{cases} \sqrt{k_0^2 - k_{mn}^2} & if\ \ k_0 > k_{mn} \\ -j\sqrt{k_{mn}^2 - k_0^2} & otherwise \end{cases}$		$\Gamma_{10}^0 = \Gamma_{01}^0 = k_0$
Modal admittance	$\xi'_{mn} = \frac{k_0}{\eta_0\Gamma_{mn}}$	$\xi''_{mn} = \frac{\Gamma_{mn}}{\eta_0 k_0}$	$\xi_{10}^0 = \xi_{01}^0 = \frac{1}{\eta_0}$

(*) TEM Floquet modes refers to the only case $\theta = 0$.

where δ_{rq} is the Kronecker delta. By substituting (2) and (3) into (6), it can be easily proved that the normalization for the potentials must be

$$\int_S \psi_r\psi_q\,dS = \delta_{rq}$$
$$\int_S \phi_r\phi_q\,dS = \delta_{rq}. \tag{7}$$

The integral equation deriving from (1) is solved by using the MoM. The magnetic currents are expressed as combinations of the magnetic modal vectors of the first Q waveguide modes

$$\vec{M}_1 = \sum_{q=1}^{Q} X_q\vec{h}_q \tag{8}$$
$$\vec{M}_2 = \sum_{q=1}^{Q} Y_q\vec{h}_q \tag{9}$$

where X_q and Y_q are unknown coefficients, and the summations extend to both TM and TE modes. By using the MoM in the Galerkin form (i.e., choosing $\vec{h}_r$ as test functions), we obtain the following matrix problem:

$$\begin{bmatrix} [A]+[B] & [C] \\ [C] & [A]+[B] \end{bmatrix}\begin{bmatrix} [X] \\ [Y] \end{bmatrix} = \begin{bmatrix} [D] \\ [0] \end{bmatrix} \tag{10}$$

where $[X]$ and $[Y]$ are the column vectors of the coefficients X_q and Y_q, $[0]$ is a null column vector of Q elements, and

$$[A]_{rq} = \sum_{m,n}\xi_{mn}\int_S \vec{h}_r\cdot\vec{\mathcal{H}}_{mn}\,dS\int_S \vec{h}_q\cdot\vec{\mathcal{H}}^*_{mn}\,dS \tag{11}$$
$$[B]_{rq} = -j\delta_{rq}y_r/\tan(\gamma_r T) \tag{12}$$
$$[C]_{rq} = j\delta_{rq}y_r/\sin(\gamma_r T) \tag{13}$$
$$[D]_r = 2\int_S \vec{h}_r\cdot\vec{H}_{\text{inc}}\,dS \tag{14}$$

where r and q range from 1 to Q, the summation in (11) extends to all types of Floquet modes (TM, TE, and, possibly, TEM), ξ_{mn} denotes the modal admittance of the Floquet modes (see Table I), and T is the thickness of the metal screen (see Fig. 3). Moreover,

$$\gamma_r = \begin{cases} \sqrt{k_0^2 - \kappa_r^2}, & \text{if } k_0 > \kappa_r \\ -j\sqrt{\kappa_r^2 - k_0^2}, & \text{otherwise} \end{cases} \tag{15}$$

is the propagation constant of the waveguide modes. In (15), $k_0 = \omega\sqrt{\epsilon_0\mu_0}$ and κ_r represents the cutoff wavenumber of a TM (κ_r') or a TE (κ_r'') mode. Furthermore, the modal admittance y_r is given by

$$y_r = \begin{cases} k_0/(\eta_0\gamma_r) & \text{TM modes} \\ \gamma_r/(\eta_0 k_0) & \text{TE modes} \end{cases} \tag{16}$$

Finally, in (14), $\vec{H}_{\rm inc}$ corresponds to $\vec{\mathcal{H}}_{01}^0$ or $\vec{\mathcal{H}}_{10}^0$ in the case of normal incidence, and to $\vec{\mathcal{H}}_{00}'$ or $\vec{\mathcal{H}}_{00}''$ in the case of oblique incidence (see Table I).

The solution of the matrix problem (10) yields the unknown coefficients X_q and Y_q. Once these coefficients have been calculated, the transmitted field $\vec{H}_{\rm tr}$ and the reflected field $\vec{H}_{\rm refl}$ can be determined. For instance, considering $\vec{H}_{\rm inc} = \vec{\mathcal{H}}_{00}'$, it results in

$$\vec{H}_{\rm tr} = \mathcal{T}_{\rm co}\vec{\mathcal{H}}_{00}' + \mathcal{T}_X\vec{\mathcal{H}}_{00}'' \tag{17}$$

$$\vec{H}_{\rm refl} = \mathcal{R}_{\rm co}\vec{\mathcal{H}}_{00}' + \mathcal{R}_X\vec{\mathcal{H}}_{00}'' \tag{18}$$

where the transmission and reflection coefficients are given by

$$\mathcal{T}_{\rm co} = \sum_{q=1}^{Q} Y_q \int_S \vec{h}_q \cdot \vec{\mathcal{H}}_{00}'\, dS \tag{19}$$

$$\mathcal{T}_X = \sum_{q=1}^{Q} Y_q \int_S \vec{h}_q \cdot \vec{\mathcal{H}}_{00}''\, dS \tag{20}$$

$$\mathcal{R}_{\rm co} = -1 + \sum_{q=1}^{Q} X_q \int_S \vec{h}_q \cdot \vec{\mathcal{H}}_{00}'\, dS \tag{21}$$

$$\mathcal{R}_X = \sum_{q=1}^{Q} X_q \int_S \vec{h}_q \cdot \vec{\mathcal{H}}_{00}''\, dS. \tag{22}$$

Similar expressions can be found when considering different incident fields (i.e., $\vec{\mathcal{H}}_{01}^0, \vec{\mathcal{H}}_{10}^0$, or $\vec{\mathcal{H}}_{00}''$).

In conclusion, the application of the MoM algorithm to the analysis of quasi-optical filters requires: 1) the evaluation of the modes of the waveguide and 2) the calculation of the coupling integrals between the waveguide modal vectors $\vec{h}_q$ and the Floquet modal vectors $\vec{\mathcal{H}}_{mn}$.

III. Determination of the Waveguide Modes by the BI-RME Method

The modes of the waveguide with a cross section S are determined by the BI-RME method [21]–[23], which is a modified version of the "Boundary Element Method" (BEM). In the BEM approach, the unknowns are current sheets defined over the boundary ∂S (Fig. 2) and acting in free space. On the contrary, in the BI-RME method, the same current sheets are embedded in an exterior rectangular resonator with a cross section Ω (Fig. 4). In fact, instead of solving directly the Helmoltz problems (4) and (5), the BI-RME method provides the solution of the "enlarged" eigenvalue problems

$$\begin{cases} \nabla_T^2\psi_r + \kappa_r'^2\psi_r = 0 & \text{in } \Omega - \partial S \\ \psi_r = 0 & \text{on } \partial\Omega \quad \text{and} \quad \partial S \end{cases} \tag{23}$$

$$\begin{cases} \nabla_T^2\phi_r + \kappa_r''^2\phi_r = 0 & \text{in } \Omega - \partial S \\ \partial\phi_r/\partial n = 0 & \text{on } \partial\Omega \quad \text{and} \quad \partial S \end{cases}. \tag{24}$$

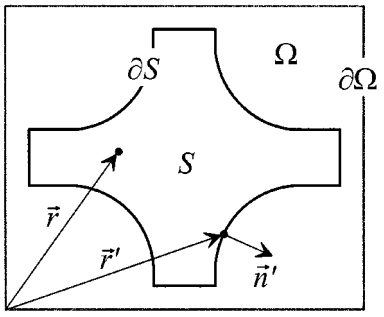

Fig. 4. The geometry considered for the application of the BI-RME method: the cross section S of the arbitrarily shaped waveguide is enclosed in the exterior rectangular resonator Ω.

Due to the introduction of the fictitious exterior rectangular resonator, the scalar potentials ψ and ϕ can be expressed in the form

$$\psi(\vec{r}) = \tilde{\psi}(\vec{r}) + \int_{\partial S} G(\vec{r},\vec{r}')f'(\vec{r}')\, d\ell' \tag{25}$$

$$\phi(\vec{r}) = \kappa''^2\tilde{\phi}(\vec{r}) - \int_{\partial S}\left[\frac{\partial F_0(\vec{r},\vec{r}')}{\partial n'} + \kappa''^2\frac{\partial F_1(\vec{r},\vec{r}')}{\partial n'}\right] f''(\vec{r}')\, d\ell' \tag{26}$$

where $\tilde{\psi}$ and $\tilde{\phi}$ are regular functions in Ω (continuously differentiables to the second order, at least) and G, F_0, and F_1 are frequency-independent Green's functions of the rectangular resonator and satisfy

$$\nabla^2 G(\vec{r},\vec{r}') = -\delta(\vec{r}-\vec{r}'), \quad \vec{r},\vec{r}' \in \Omega \tag{27}$$

$$G(\vec{r},\vec{r}') = 0, \quad \vec{r} \in \partial\Omega \tag{28}$$

$$\nabla^2 F_0(\vec{r},\vec{r}') = -\delta(\vec{r}-\vec{r}') + 1/\Omega, \quad \vec{r},\vec{r}' \in \Omega \tag{29}$$

$$\nabla^2 F_1(\vec{r},\vec{r}') = -F_0(\vec{r},\vec{r}'), \quad \vec{r},\vec{r}' \in \Omega \tag{30}$$

$$\frac{\partial F_0}{\partial n_\Omega} = \frac{\partial F_1}{\partial n_\Omega} = 0, \quad \vec{r} \in \partial\Omega \tag{31}$$

$$\int_\Omega F_0\, d\Omega = \int_\Omega F_1\, d\Omega = 0 \tag{32}$$

where $\vec{n}_\Omega$ is the outward normal vector on $\partial\Omega$.

Thus, integrals in (25) and (26) represent the quasi-static potentials produced in Ω by an equivalent source density f' or f'' located on ∂S, respectively; f' and f'' represent (apart from scale factors) the longitudinal current density of the TM modes and the transverse current density of the TE modes, respectively.

Note, that due to the above-mentioned regularity of $\tilde{\psi}$ and of $\tilde{\phi}$ (i.e., the continuity of $\partial\tilde{\psi}/\partial n$ and of $\tilde{\phi}$ across ∂S), the discontinuity of $\partial\psi/\partial n$ and of ϕ resides on the integrals appearing in (25) and (26). Therefore, for a well-known property of Green's integrals, the discontinuities of $\partial\psi/\partial n$ and ϕ coincide with f' and f'', respectively

$$\frac{\partial\psi^-(\vec{r})}{\partial n} - \frac{\partial\psi^+(\vec{r})}{\partial n} = f'(\vec{r}) \quad \text{on } \partial S \tag{33}$$

$$\phi^-(\vec{r}) - \phi^+(\vec{r}) = f''(\vec{r}) \quad \text{on } \partial S \tag{34}$$

where $+$ and $-$ denote quantities taken on the external and internal side of ∂S.

By substituting (25) into (23), we obtain the following system of two integro-differential equations for the TM scalar potentials [22]:

$$\begin{cases} \nabla^2\tilde{\psi}(\vec{r}) + \kappa'^2[\tilde{\psi}(\vec{r}) \\ \quad + \int_{\partial S} G(\vec{r},\vec{r}')f'(\vec{r}')\,d\ell'] = 0, \quad \vec{r}\in\Omega \\ \tilde{\psi}(\vec{r}) + \int_{\partial S} G(\vec{r},\vec{r}')f'(\vec{r}')\,d\ell' = 0, \quad \vec{r}\in\partial S \end{cases}. \tag{35}$$

Analogously, by substituting (26) into (24) and exploiting the properties of Green's functions, we obtain the corresponding system for the TE scalar potentials [23]

$$\begin{cases} \nabla^2\tilde{\phi}(\vec{r}) + \kappa''^2\left[\tilde{\phi}(\vec{r}) \right. \\ \quad \left. - \int_{\partial S} \frac{\partial F_1(\vec{r},\vec{r}')}{\partial n'} f''(\vec{r}')d\ell'\right] = 0, \quad \vec{r}\in\Omega \\ \kappa''^2\left[\frac{\partial\tilde{\phi}(\vec{r})}{\partial n} - \int_{\partial S}\frac{\partial^2 F_1(\vec{r},\vec{r}')}{\partial n\partial n'} f''(\vec{r}')d\ell'\right] \\ \quad -\frac{\partial}{\partial t}\int_{\partial S} G(\vec{r},\vec{r}')\frac{\partial f''(\vec{r}')}{\partial t'}\,d\ell' = 0, \quad \vec{r}\in\partial S \end{cases}. \tag{36}$$

Equations (35) and (36) constitute linear eigenvalue problems involving the unknowns $\{f', \tilde{\psi}\}$ and $\{f'', \tilde{\phi}\}$, respectively. Their solutions are obtained by using the MoM.

The boundary ∂S is approximated by a polygonal line with segment length not exceeding a quarter wavelength at the maximum frequency of interest, and the functions f' and f'' are approximated using suitable basis functions α_p and β_p (e.g., piecewise-parabolic splines, as discussed in [21, Sec. 5.2.4])

$$f'(\vec{r}') = \sum_p a_p\alpha_p(\vec{r}') \tag{37}$$

$$f''(\vec{r}') = \sum_p b_p\beta_p(\vec{r}') \tag{38}$$

and, thanks to their regularity, functions $\tilde{\psi}$ and $\tilde{\phi}$ can be represented as resonant mode expansions

$$\tilde{\psi}(\vec{r}) = \sum_i c_i\Psi_i(\vec{r}) \tag{39}$$

$$\tilde{\phi}(\vec{r}) = \sum_i d_i\Phi_i(\vec{r}) \tag{40}$$

involving the potentials Ψ and Φ of the first TM and TE modes of the rectangular resonator Ω, respectively [21, p. 336].

By substituting (37) and (39) into (35), and (38) and (40) into (36), and applying Galerkin's method, we obtain two linear matrix eigenvalue problems, the first one for the TM modes and the second one for the TE modes. The eigensolutions of (35) and (36) are the cutoff wavenumbers κ'_q and κ''_q, and the coefficients $a_p^{(q)}, b_p^{(q)}, c_i^{(q)}$, and $d_i^{(q)}$, where the index q refers to the qth TM or TE mode.

More details on the numerical implementation of the BI-RME method (i.e., the analytical espressions of the basis functions as well as of the potentials Φ_i and Ψ_i, the expressions of the entries of the eigenvalue problem matrices, the analytical expressions of G, F_0, and F_1 in terms of rapidly convergent one-index series, the numerical approach for the calculation of the matrices, etc.) are available in [21]–[23] and are not reported here since their discussion is beyond the scope of this work.

It is worth observing that, by solving (23) and (24), we find not only the required solutions (i.e., those pertaining to the domain S), but also the solutions pertaining to the domain $\Omega - S$. However, these "spurious" solutions can be easily selected and discarded (see [21, Sec. 5.2.5]). Hence, although (25) and (26) define the potentials in the domain Ω, the eigenfunctions ψ_q and ϕ_q of the qth TM or TE mode, calculated by the BI-RME method, practically vanish in $\Omega - S$ so that they are automatically normalized according to (7) [22], [23]. Moreover, $\partial\psi_q^+/\partial n = 0$ and $\phi_q^+ = 0$ on ∂S, so that (33) and (34) become

$$\frac{\partial\psi_q(\vec{r})}{\partial n} = f'_q(\vec{r}) = \sum_p a_p^{(q)}\alpha_p(\vec{r}) \quad \text{on } \partial S \tag{41}$$

$$\phi_q(\vec{r}) = f''_q(\vec{r}) = \sum_p b_p^{(q)}\beta_p(\vec{r}) \quad \text{on } \partial S. \tag{42}$$

As will be shown later, the evaluation of the potentials (25) and (26) and of the corresponding modal vectors (2) and (3) needed in the calculation of (11) and (14) can be avoided, by obtaining the MoM matrices using directly (41) and (42), and, therefore, from the knowledge of $a_p^{(q)}$ and $b_p^{(q)}$.

IV. Calculation of the Coupling Integrals

The evaluation of (11) requires the calculation of the "coupling integrals"

$$\int_S \vec{h}_q\cdot\vec{\mathcal{H}}^*_{mn}\,dS \tag{43}$$

for all six combinations of TE or TM waveguide modes with the TE, TM, or TEM Floquet modes. The other integral appearing in (11) is the conjugate of (43). Moreover, as discussed in Section II, the incident field $\vec{H}_{\rm inc}$ in (14) represents a Floquet modal vector (i.e., $\vec{\mathcal{H}}^0_{10}, \vec{\mathcal{H}}^0_{01}, \vec{\mathcal{H}}'_{00}$ or $\vec{\mathcal{H}}''_{00}$), depending on the angle of incidence and on the polarization of the impinging wave. Thus, also the integral in (14) reduces to (43).

Integral (43) could be directly calculated by a numerical surface integration, using the expression of the potentials (25) and (26) together with (2) and (3), and expressions of the Floquet modal fields reported in Table I. Nevertheless, a substantial improvement in computational efficiency can be achieved by transforming the surface integrals into contour integrals. In fact, as derived in the Appendix, we have

$$\int_S \vec{h}'_q\cdot\vec{\mathcal{H}}'^*_{mn}\,dS = \frac{k_{mn}}{\kappa'_q\left(k_{mn}^2-\kappa_q'^2\right)}\int_{\partial S}\frac{\partial\psi_q}{\partial n}\chi^*_{mn}\,d\ell \tag{44}$$

$$\int_S \vec{h}'_q\cdot\vec{\mathcal{H}}''^*_{mn}\,dS = 0 \tag{45}$$

$$\int_S \vec{h}'_q\cdot\vec{\mathcal{H}}^{0*}_{mn}dS = 0 \tag{46}$$

$$\int_S \vec{h}''_q\cdot\vec{\mathcal{H}}'^*_{mn}\,dS = -\frac{1}{\kappa''_q k_{mn}}\int_{\partial S}\phi_q\frac{\partial\chi^*_{mn}}{\partial t}\,d\ell \tag{47}$$

$$\int_S \vec{h}''_q\cdot\vec{\mathcal{H}}''^*_{mn}\,dS = \frac{\kappa''_q}{k_{mn}\left(\kappa_q''^2-k_{mn}^2\right)}\int_{\partial S}\phi_q\frac{\partial\chi^*_{mn}}{\partial n}\,d\ell \tag{48}$$

$$\int_S \vec{h}''_q\cdot\vec{\mathcal{H}}^{0*}_{mn}\,dS = -\frac{1}{\kappa''_q}\int_{\partial S}\phi_q\frac{\partial\chi^0_{mn}}{\partial t}\,d\ell. \tag{49}$$

In (47) and (49), the derivatives are taken with respect to the tangent vector $\vec{t}$ indicated in Fig. 2.

The apparent advantage of this transformation comes from the possibility of calculating the coupling integrals by a one-dimensional (1-D) numerical integration. Furthermore, observing that the contour integrals involve $\partial\psi_q/\partial n$ and ϕ_q, which are given by (41) and (42) as a by-product of the BI-RME analysis, by substituting (41) and (42) into (44) and (47)–(49), we obtain

$$\int_S \vec{h}'_q \cdot \vec{\mathcal{H}}'^*_{mn}\, dS = \frac{k_{mn}}{\kappa'_q\left(k_{mn}^2 - \kappa_q'^2\right)} \sum_p a_p^{(q)} \int_{\partial S} \alpha_p \chi^*_{mn}\, d\ell \tag{50}$$

$$\int_S \vec{h}''_q \cdot \vec{\mathcal{H}}''^*_{mn}\, dS = -\frac{1}{\kappa''_q\, k_{mn}} \sum_p b_p^{(q)} \int_{\partial S} \beta_p \frac{\partial \chi^*_{mn}}{\partial t}\, d\ell \tag{51}$$

$$\int_S \vec{h}''_q \cdot \vec{\mathcal{H}}''^*_{mn}\, dS = \frac{\kappa''_q}{k_{mn}\left(\kappa_q''^2 - k_{mn}^2\right)} \sum_p b_p^{(q)} \int_{\partial S} \beta_p \frac{\partial \chi^*_{mn}}{\partial n}\, d\ell \tag{52}$$

$$\int_S \vec{h}''_q \cdot \vec{\mathcal{H}}^{0*}_{mn}\, dS = -\frac{1}{\kappa''_q} \sum_p b_p^{(q)} \int_{\partial S} \beta_p \frac{\partial \chi^0_{mn}}{\partial t}\, d\ell. \tag{53}$$

Since the integrals in (50)–(53) can be calculated analytically, the use of the BI-RME method leads to a dramatic computational advantage.

Finally, it is worth observing that, in cases where $\kappa_q^2 = k_{mn}^2$, (50) and (52) are not applicable and the surface integration is required.

V. Numerical and Experimental Results

The algorithm described in the previous sections has been implemented in a computer code. To demonstrate the capabilities of the code, we present the analysis of two structures: a dichroic mirror operating in the X-band and a quasi-optical bandpass filter operating in the mm-wave region.

The first example refers to the analysis of the X-band dichroic filter reported in [24], consisting of a metal plate perforated with cross-shaped apertures (Fig. 5). In this structure, the thickness $T = 31.8$ mm of the metal plate is comparable with the wavelength and the angle of incidence is oblique $(\theta = 30°, \phi = 0°)$.

A possible approach to the analysis of dichroic plates perforated with crosses, which was adopted in [24], is based on the hypothesis that the thickness w (see Fig. 5) of the metal wall separating the apertures is zero. Under this hypothesis, the currents on the front and back faces of the plate were neglected, and the solution was found by an integral equation method, solved by using the MoM: rooftop basis and razor testing functions were applied. Though efficient, this approach is limited, because the effect of the metal walls is small but not negligible and plays an important role in the resonance frequencies. Moreover, this analysis is limited to cross-shaped holes defined by a sharp contour. It is not possible, for instance, to take into account the unavoidable rounded corners due to the manufacturing process.

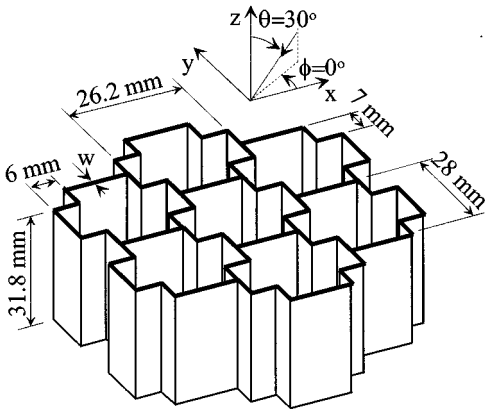

Fig. 5. Schematic representation of the X-band dichroic filter. In the prototype, the wall thickness was $w = 0.41$ mm. The angle of incidence is $\theta = 30°$, $\phi = 0°$.

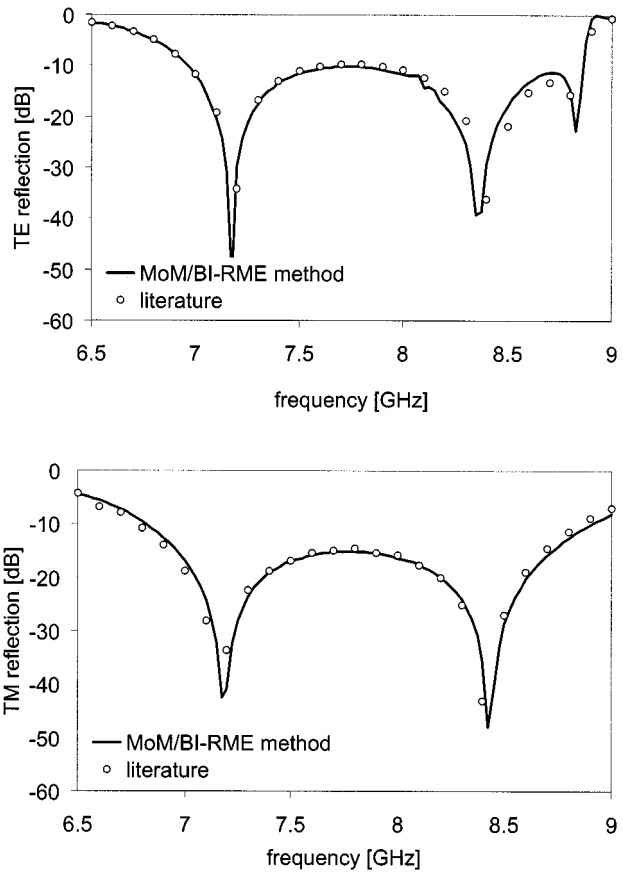

Fig. 6. Analysis of the X-band dichroic filter with infinitely thin metal walls $(w = 0)$: MoM/BI-RME analysis is compared with simulations reported in the literature.

By using the MoM/BI-RME method, we performed the analysis of the dichroic filter, both under the hypothesis of $w = 0$ and considering the actual thickness $w = 0.41$ mm. The analysis of the dichroic plate with infinitely thin metal walls is reported in Fig. 6 and compared with the simulations reported in [24]. Conversely, the analysis of the dichroic plate with finite

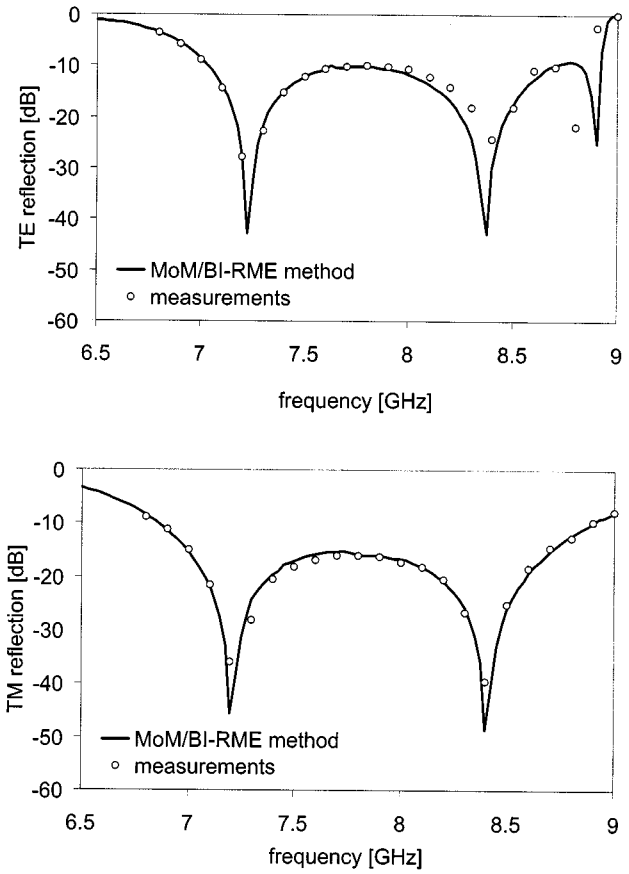

Fig. 7. Analysis of the X-band dichroic filter with metal walls of finite thickness ($w = 0.41$ mm): MoM/BI-RME analysis is compared with measurements reported in the literature.

metal walls is reported in Fig. 7 and compared with the experimental results reported in [24]. The agreement between our simulation and the measurements is very good, for both TM and TE polarization. In the analysis, we used 34 entire domain basis functions and 400 Floquet modes, in the case of both infinitely thin and thick metal walls. The simulation required 62 s on a PC Pentium III 600 MHz for the analysis in 100 frequency points in the band 6.5–9 GHz. The numerical convergence of the method was checked by increasing the number of basis functions and Floquet modes. No significant change in the frequency response was observed.

The second example refers to the analysis of a quasi-optical bandpass filter, operating at 280 GHz [25]. It consists of a free-standing copper foil with a thickness $T = 10$ μm, perforated periodically with cross-shaped apertures (see photographs in Fig. 8). The geometrical dimensions of the filter are reported in Fig. 9. This filter was fabricated at the University of Erlangen by galvanizing growth on a base substrate [26] and measured at the University of Freiburg by terahertz time-domain spectroscopy [27]. Details related to technological issues are widely discussed in [28]. The filter was excited by a uniform plane wave, incident from the broadside direction $(\theta = 0)$ and linearly polarized along the y direction.

As a first step, the analysis was performed up to 1.6 THz by considering the nominal values of the geometrical dimensions, i.e., considering the sharp corners in the aperture boundary

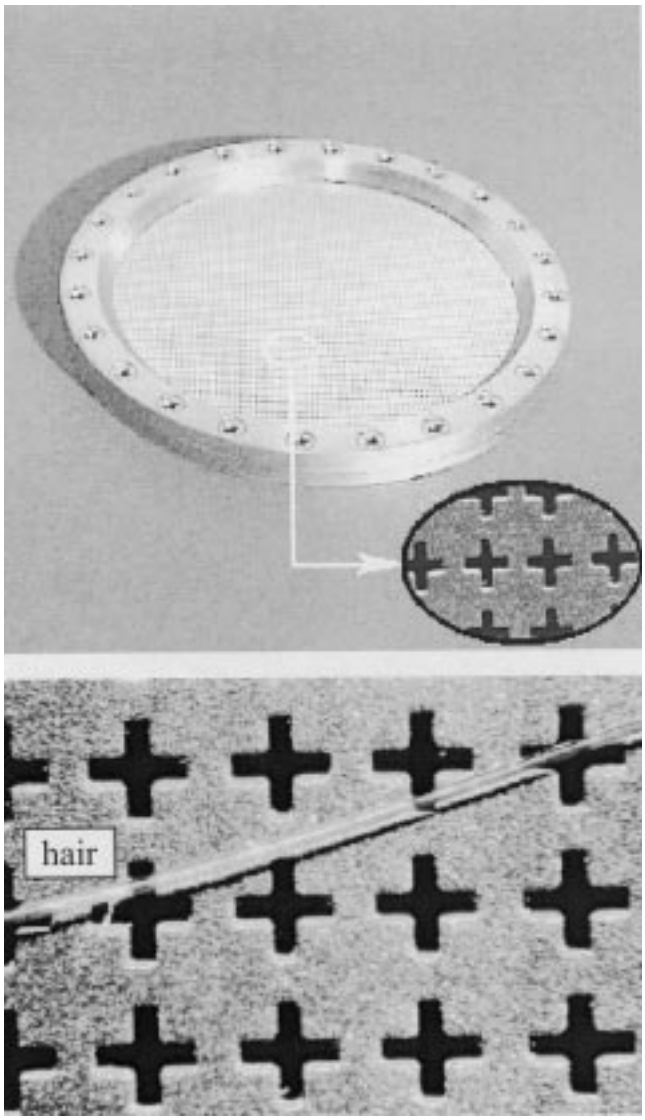

Fig. 8. Photographs of the 280-GHz quasi-optical filter.

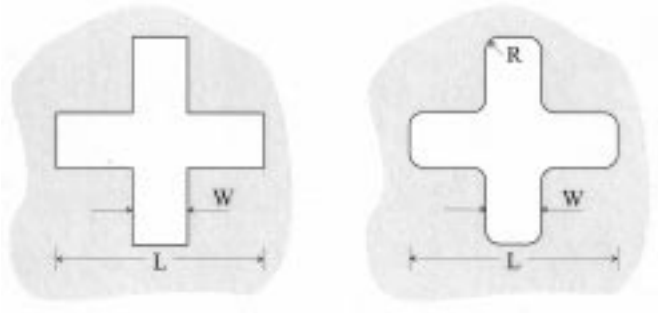

(a) (b)

Fig. 9. Geometry of the aperture of the quasi-optical filter: (a) the cross with sharp corners snf (b) the cross with rounded corners. The dimensions of the aperture and the periodicity are: $L = 570$ μm, $W = 160$ μm, $R = 40$ μm, $a = b = 810$ μm, and $\alpha = 90°$.

[Fig. 9(a)]. The convergence of the method was achieved with 31 waveguide modes and 400 Floquet modes. The computing time (on a PC Pentium III 600 MHz) was 10 s for the (frequency-independent) determination of the waveguide modes by the BI-RME method, and 0.6 s for the calculation of the

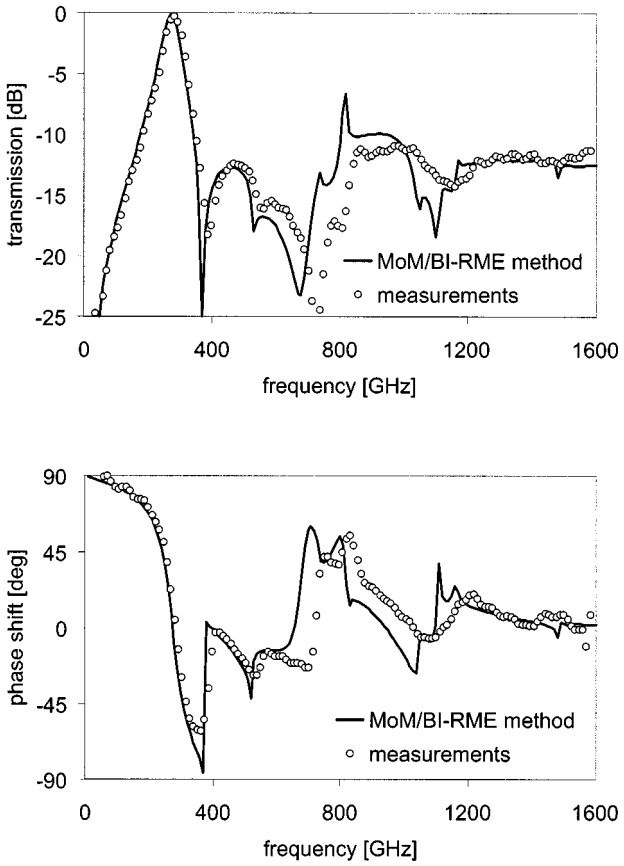

Fig. 10. Numerical results for the filter considering the aperture shape with sharp corners [Fig. 9(a)], compared with experimental data. The transmittance phase is the difference between the phase measured with and without the filter.

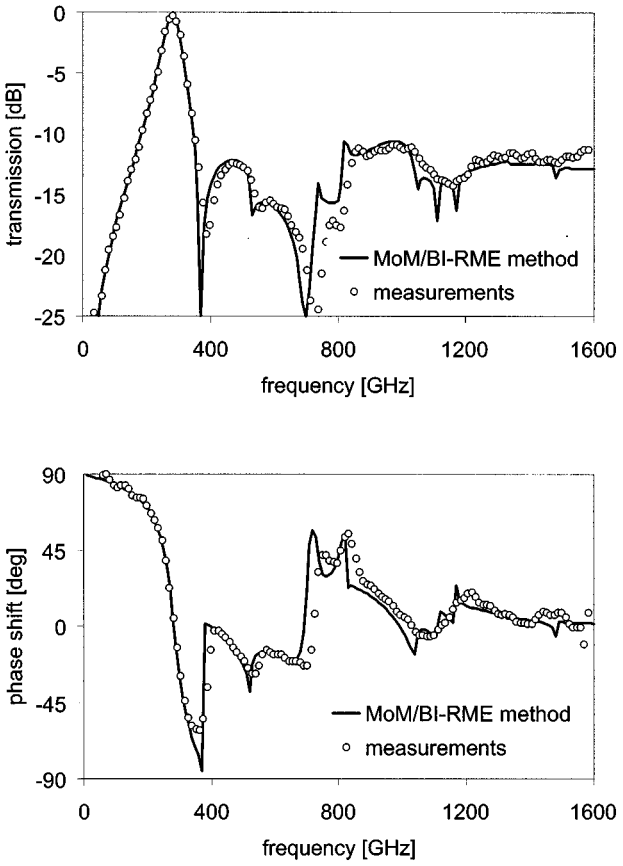

Fig. 11. Numerical results for the filter considering the aperture shape with rounded corners [Fig. 9(b)], compared with experimental data.

transmission/reflection coefficients on each frequency point. Therefore, the analysis on 160 frequency points in the band 10–1600 GHz required 106 s. The results of the analysis are shown in Fig. 10, together with the measured data. The agreement between simulations and measurements is quite good, the only discrepancy being a small shift in the predicted resonance frequency, which was approximately 4% lower than the measured one.

This frequency shift is due to the unavoidable smoothness of the aperture boundary, resulting from the fabrication process. From the photomicrographs, it can be deduced that an arc of radius $R = 40\ \mu$m should be considered instead of the sharp corners. Hence, we simulated the filter considering the cross section drawn in Fig. 9(b). The number of basis functions (waveguide modes) as well as Floquet modes did not change with respect to the previous simulation and, consequently, the computing time was identical. However, the resonance frequency of the filter shifted upward, getting closer to the measured one (Fig. 11) and reducing the error to 0.7%. The agreement between the simulations and the experimental data is excellent in the whole frequency band, both considering the magnitude and the phase.

As a final remark, we would like to point out that the analyses presented above did not take advantage of the symmetries of the problems, which are related to the aperture shape in conjunction with the particular direction and polarization of the incident wave. Considering the symmetries dramatically reduces the CPU times. In fact, only those modes satisfying the proper symmetry conditions are excited by the incident field. This leads to a number of advantages.

- The calculation of the waveguide modes by the BI-RME method can be performed by exploiting the symmetries, thus reducing the computing time [21].
- The selection by symmetry of the waveguide modes causes a reduction in the dimension of the matrix problem (10), which must be solved frequency-by-frequency.
- The number of Floquet modes involved in the calculation of the MoM matrix (11) is reduced.
- In the case of normal incidence, the Floquet modes are frequency-independent, and, therefore, the evaluation of the coupling integrals (44)–(49) can be performed only once, before starting the frequency sweep.

VI. Conclusion

This paper presented a fast and accurate CAD tool for the analysis of quasi-optical filters, consisting of a thick metal screen perforated periodically with arbitrarily shaped holes. The code implements an algorithm based on a hybrid MoM/BI-RME method. The use of the BI-RME method permits an efficient determination of the waveguide modes used as entire domain basis functions in the MoM analysis. Moreover, the transformation of the surface integrals appearing in the

MoM matrices into line integrals permits their calculation using quantities obtained as a by-product of the BI-RME analysis.

The analysis of two quasi-optical filters operating at 8 GHz and 280 GHz was presented. In both cases, the simulations and the experimental data show an excellent agreement in a wide frequency band. Moreover, by exploiting the peculiarities of the BI-RME method in the analysis of the filter at 280 GHz, we accounted for the smoothness of the aperture shape due to the manufacturing process.

The typical computing time on a standard PC was of the order of tens of seconds for the analysis of the filters in the whole frequency band. This time is orders of magnitude shorter than the one required by a commercial code considered for comparison. Moreover, at least in the case of normal incidence, it can be considerably reduced by exploiting the symmetries of the structure.

APPENDIX

The transformation from surface to line integrals is based on the application of Green's identity (see, for instance, [29, Appendix 2, eq. (45)])

$$\int_S \vec{\mathcal{A}} \cdot \nabla_T \mathcal{B}\, dS = \int_{\partial S} \mathcal{B}\vec{n} \cdot \vec{\mathcal{A}}\, d\ell - \int_S \mathcal{B}\nabla_T \cdot \vec{\mathcal{A}}\, dS. \quad \text{(A1)}$$

Derivation of (44): The magnetic modal fields are related to the potentials (see Table I and (2)), thus resulting in

$$\int_S \vec{h}'_q \cdot \vec{\mathcal{H}}'^*_{mn}\, dS = \int_S \vec{u}_z \times \frac{\nabla_T \psi_q}{\kappa'_q} \cdot \vec{u}_z \times \frac{\nabla_T \chi^*_{mn}}{k_{mn}}\, dS = \frac{1}{\kappa'_q k_{mn}} \int_S \nabla_T \psi_q \cdot \nabla_T \chi^*_{mn}\, dS. \quad \text{(A2)}$$

By applying (A1) to (.2) with $\vec{\mathcal{A}} = \nabla_T \chi^*_{mn}$ and $\mathcal{B} = \psi_q$, and substituting $\nabla^2_T \chi_{mn} = -k^2_{mn}\chi_{mn}$ (see Table I), we have

$$\int_S \vec{h}'_q \cdot \vec{\mathcal{H}}'^*_{mn}\, dS = \frac{1}{\kappa'_q k_{mn}} \int_{\partial S} \psi_q \vec{n} \cdot \nabla_T \chi^*_{mn}\, d\ell + \frac{k_{mn}}{\kappa'_q} \int_S \psi_q \chi^*_{mn}\, dS. \quad \text{(A3)}$$

Moreover, by choosing $\vec{\mathcal{A}} = \nabla_T \psi_q$ and $\mathcal{B} = \chi^*_{mn}$, taking into account that $\nabla^2_T \psi_q = -\kappa'^2_q \psi_q$, and applying (A1) to (A2), we have

$$\int_S \vec{h}'_q \cdot \vec{\mathcal{H}}'^*_{mn}\, dS = \frac{1}{\kappa'_q k_{mn}} \int_{\partial S} \chi^*_{mn} \vec{n} \cdot \nabla_T \psi_q\, d\ell + \frac{\kappa'_q}{k_{mn}} \int_S \psi_q \chi^*_{mn}\, dS. \quad \text{(A4)}$$

By substituting the surface integral into the right-hand side of (A4) into (A3), considering $\kappa'^2_q \neq k^2_{mn}$ and remembering that $\psi_q = 0$ on ∂S, we finally obtain (44).

Derivation of (45) and (46): From Table I and (2), we have

$$\int_S \vec{h}'_q \cdot \vec{\mathcal{H}}''^*_{mn}\, dS = \int_S \vec{u}_z \times \frac{\nabla_T \psi_q}{\kappa'_q} \cdot \frac{\nabla_T \chi^*_{mn}}{k_{mn}}\, dS = -\frac{1}{\kappa'_q k_{mn}} \int_S \nabla_T \psi_q \cdot \vec{u}_z \times \nabla_T \chi^*_{mn}\, dS. \quad \text{(A5)}$$

By applying (A1) to (A5) with $\vec{\mathcal{A}} = \vec{u}_z \times \nabla_T \chi^*_{mn}$ and $\mathcal{B} = \psi_q$, we have

$$\int_S \vec{h}'_q \cdot \vec{\mathcal{H}}''^*_{mn}\, dS = -\frac{1}{\kappa'_q k_{mn}} \int_{\partial S} \psi_q \vec{n} \cdot \vec{u}_z \times \nabla_T \chi^*_{mn}\, d\ell + \frac{1}{\kappa'_q k_{mn}} \int_S \psi_q \nabla_T \cdot (\vec{u}_z \times \nabla_T \chi^*_{mn})\, dS. \quad \text{(A6)}$$

In the right-hand side of (A6), the line integral vanishes since $\psi_q = 0$ on ∂S, whereas the surface integral vanishes because

$$\nabla_T \cdot (\vec{u}_z \times \nabla_T \mathcal{F}) = 0 \quad \text{(A7)}$$

for any scalar function $\mathcal{F}$ (see, for instance, [29, Appendix 2, eq. (38)]).

In a similar way, we derive (46).

Derivation of (47): From Table I and (3), we obtain

$$\int_S \vec{h}''_q \cdot \vec{\mathcal{H}}'^*_{mn}\, dS = \frac{1}{\kappa''_q k_{mn}} \int_S \nabla_T \phi_q \cdot \vec{u}_z \times \nabla_T \chi^*_{mn}\, dS. \quad \text{(A8)}$$

By applying (A1) to (A8) with $\vec{\mathcal{A}} = \vec{u}_z \times \nabla_T \chi^*_{mn}$ and $\mathcal{B} = \phi_q$, we have

$$\int_S \vec{h}''_q \cdot \vec{\mathcal{H}}'^*_{mn}\, dS = \frac{1}{\kappa''_q k_{mn}} \int_{\partial S} \phi_q \vec{n} \cdot \vec{u}_z \times \nabla_T \chi^*_{mn}\, d\ell - \frac{1}{\kappa''_q k_{mn}} \int_S \phi_q \nabla_T \cdot (\vec{u}_z \times \nabla_T \chi^*_{mn})\, dS. \quad \text{(A9)}$$

The surface integral in the right-hand side of (A9) vanishes due to (A7). Moreover, by considering that $\vec{n} \cdot \vec{u}_z \times \nabla_T \chi^*_{mn} = -\partial \chi^*_{mn}/\partial t$ (where $\vec{t}$ is defined in Fig. 2), we obtain (47).

Derivation of (48): By substituting the magnetic modal fields with their expression in terms of scalar potentials (see Table I and (3)), we obtain

$$\int_S \vec{h}''_q \cdot \vec{\mathcal{H}}''^*_{mn}\, dS = \frac{1}{\kappa''_q} \int_S \nabla_T \phi_q \cdot \nabla_T \chi^{0*}_{mn}\, dS. \quad \text{(A10)}$$

Therefore, the derivation of (48) is similar to the one of (44), only taking into account the different boundary condition of the waveguide scalar potential.

Derivation of (49): From Table I and (3), we obtain

$$\int_S \vec{h}''_q \cdot \vec{\mathcal{H}}^{0*}_{mn}\, dS = \frac{1}{\kappa''_q} \int_S \nabla_T \phi_q \cdot \vec{u}_z \times \nabla_T \chi^{0*}_{mn}\, dS. \quad \text{(A11)}$$

By applying (A1) to (A11) with $\vec{\mathcal{A}} = \vec{u}_z \times \nabla_T \chi^{0*}_{mn}$ and $\mathcal{B} = \phi_q$, we have

$$\int_S \vec{h}''_q \cdot \vec{\mathcal{H}}^{0*}_{mn}\, dS = \frac{1}{\kappa''_q} \int_{\partial S} \phi_q \vec{n} \cdot \vec{u}_z \times \nabla_T \chi^{0*}_{mn}\, d\ell - \frac{1}{\kappa''_q} \int_S \phi_q \nabla_T \cdot \vec{u}_z \times \nabla_T \chi^{0*}_{mn}\, dS. \quad \text{(A12)}$$

In the right-hand side of (A12), the surface integral vanishes due to (A7), and $\vec{n} \cdot \vec{u}_z \times \nabla_T \chi^{0*}_{mn} = -\partial \chi^0_{mn}/\partial t$. This proves (49).

ACKNOWLEDGMENT

The authors gratefully acknowledge Prof. G. Conciauro for his valuable suggestions.

REFERENCES

[1] T. K. Wu, *Frequency Selective Surface and Grid Array*. New York: Wiley, 1995.
[2] J. C. Vardaxoglou, *Frequency Selective Surfaces*. New York: Wiley, 1997.
[3] B. A. Munk, *Frequency Selective Surfaces: Theory and Design*. New York: Wiley Interscience, 2000.
[4] R. Mittra, C. H. Chan, and T. Cwik, "Techniques for analyzing frequency selective surfaces—A review," *Proc. IEEE*, vol. 76, pp. 1593–1615, Dec. 1988.
[5] C. C. Chen, "Transmission of microwave through perforated flat plates of finite thickness," *IEEE Trans. Microwave Theory Tech.*, vol. MTT-21, pp. 1–6, Jan. 1973.
[6] P. Harms, R. Mittra, and K. Wai, "Implementation of the periodic boundary condition in the finite-difference time-domain algorithm for FSS structures," *IEEE Trans. Antennas Propagat.*, vol. 42, pp. 1317–1324, Sept. 1994.
[7] M. Lambea, M. A. Gonzalez, J. A. Encinar, and J. Zapata, "Analysis of frequency selective surfaces with arbitrarily shaped apertures by finite element method and generalized scattering matrix," in *IEEE APS Int. Symp. 1995 Digest*, 1995, pp. 1644–1647.
[8] E. W. Lucas and T. P. Fontana, "A 3-D hybrid finite element/boundary element method for the unified radiation and scattering analysis of general infinite periodic arrays," *IEEE Trans. Antennas Propagat.*, vol. 43, pp. 145–153, Feb. 1995.
[9] T. F. Eibert and J. L. Volakis, "Adaptive integral method for hybrid FE/BI modeling of 3D doubly periodic structures," in *IEEE Antennas and Propagation Soc. Int. Symp. 1998 Dig.*, 1998, pp. 1754–1757.
[10] T. F. Eibert, J. L. Volakis, D. R. Wilton, and D. R. Jackson, "Hybrid FE/BI modeling of 3-D doubly periodic structures utilizing triangular prismatic elements and an MPIE formulation accelerated by the Ewald transformation," *IEEE Trans. Antennas Propagat.*, vol. 47, pp. 843–850, May 1999.
[11] T. F. Eibert and J. L. Volakis, "Fast spectral domain algorithm for hybrid finite element/boundary integral modeling of infinite periodic arrays," in *IEEE Antennas and Propagation Soc. Int. Symp. 1999 Dig.*, 1999, pp. 1206–1209.
[12] T. Cwik, S. Fernandez, A. Ksendzov, C. C. La Baw, P. D. Maker, and R. E. Muller, "Multi-bandwidth frequency selective surfaces for near infrared filtering: Design and optimization," in *IEEE Antennas and Propagation Soc. Int. Symp. 1999 Dig.*, 1999, pp. 1726–1729.
[13] M. Bozzi and L. Perregrini, "Efficient analysis of thin conductive screens perforated periodically with arbitrarily shaped apertures," *Electron. Lett.*, vol. 35, no. 13, pp. 1085–1087, June 1999.
[14] ——, "Efficient analysis of frequency selective surfaces by the method of moments with entire domain basis functions," in *Proc. ECCOMAS 2000*, Barcelona, Catalonia, Spain, Sept. 11–14, 2000.
[15] E. L. Pelton and B. A. Munk, "Scattering from periodic arrays of cross dipoles," *IEEE Trans. Antennas Propagat.*, vol. AP-27, pp. 323–330, Mar. 1979.
[16] C. H. Tsao and R. Mittra, "Spectral-domain analysis of frequency selective surfaces comprised of periodic arrays of cross dipoles and Jerusalem crosses," *IEEE Trans. Antennas Propagat.*, vol. AP-32, pp. 478–486, May 1984.
[17] E. L. Pelton and B. A. Munk, "A streamlined metallic radome," *IEEE Trans. Antennas Propagat.*, vol. AP-22, pp. 799–803, June 1974.
[18] J. C. Vardaxoglou and E. A. Parker, "Performance of two tripole arrays as frequency selective surfaces," *Electron. Lett.*, vol. 19, no. 18, pp. 709–710, Sept. 1983.
[19] J. Huang, T. K. Wu, and S. W. Lee, "Tri-band frequency selective surface with circular ring elements," *IEEE Trans. Antennas Propagat.*, vol. 42, pp. 166–175, Feb. 1994.
[20] T. K. Wu, "Single-screen triband frequency selective surface with double-square-loop elements," *Microwave Opt. Technol. Lett.*, vol. 5, no. 2, pp. 56–59, Feb. 1992.
[21] G. Conciauro, M. Guglielmi, and R. Sorrentino, *Advanced Modal Analysis*. New York: Wiley, 2000.
[22] G. Conciauro, P. Arcioni, M. Bressan, and L. Perregrini, "Wideband modeling of arbitrarily shaped H-plane waveguide components by the 'boundary integral-resonant mode expansion method'," *IEEE Trans. Microwave Theory Tech.*, vol. 44, pp. 1057–1066, July 1996.
[23] P. Arcioni, M. Bressan, G. Conciauro, and L. Perregrini, "Wideband modeling of arbitrarily shaped E-plane waveguide components by the 'boundary integral-resonant mode expansion method'," *IEEE Trans. Microwave Theory Tech.*, vol. 44, pp. 2083–2092, Nov. 1996.
[24] L. W. Epp, P. H. Stanton, R. E. Jorgenson, and R. Mittra, "Experimental verification of an integral equation solution for a thin-walled dichroic plate with cross-shaped holes," *IEEE Trans. Antennas & Propagat.*, vol. 42, pp. 878–882, June 1994.
[25] C. Winnewisser, F. Lewen, J. Weinzierl, and H. Helm, "Frequency-selective surfaces analyzed by THz-time-domain spectroscopy," in *1998 IEEE 6th Int. Conf. on THz Electronics Proc.*, Leeds, U.K., Sept. 2–3, 1998, pp. 196–198.
[26] D. Steup and J. Weinzierl, "Resonant THz-meshes," in *Proc. 4th Int. THz Workshop*, Erlangen-Tennenlohe, Germany, Sept. 5–6, 1996.
[27] C. Winnewisser, F. Lewen, and H. Helm, "Transmission characteristics of dichroic filters measured by THz time-domain spectroscopy," *Appl. Phys. A*, vol. 66, pp. 593–598, 1998.
[28] M. Bozzi, L. Perregrini, J. Weinzierl, and C. Winnewisser, "Design, fabrication, and measurement of frequency selective surfaces," *Opt. Eng.*, vol. 39, no. 8, pp. 2263–2269, Aug. 2000.
[29] J. Van Bladel, *Electromagnetic Fields*. Washington, DC: Hemisphere, 1985.

Maurizio Bozzi (S'98–M'01) was born in Voghera, Italy, in 1971. He received the "Laurea" degree in electronic engineering and the Ph.D. in electronics and computer science from the University of Pavia, Pavia, Italy, in 1996 and 2000, respectively.

From December 1996 to September 1997, he was a guest researcher at the Technische Universität Darmstadt, Germany, in the framework of a European TMR project. His main research activities concern the electromagnetic modeling of frequency selective surfaces, quasi-optical frequency multipliers, and microwave printed and integrated circuits.

Dr. Bozzi was awarded the MECSA prize for the best paper presented by a young researcher at the 2000 Italian Conference on Electromagnetics (XIII RINEM). He is a member of the Society of Photo-Optical Instrumentation Engineers (SPIE) and a Correspondent of the International Union of Radio Science (URSI).

Luca Perregrini (M'98) was born in Sondrio, Italy, in 1964. He graduated in electronic engineering and received the Ph.D. degree in electronics and computer science from the University of Pavia, Pavia, Italy, in 1989 and 1993, respectively.

In 1992, he joined the Department of Electronics of the University of Pavia as an Assistant Professor in electromagnetics and has held a course in Electromagnetic Field Theory since 1996. His current research interests are in numerical methods for the analysis and optimization of waveguide circuits, in the electromagnetic modeling of quasi-optical circuits (frequency multipliers and frequency selective surfaces) in the millimeter and sub-millimeter wave range, and in the modeling of microwave printed and integrated circuits.

Jochen Weinzierl was born in Nürnberg, Germany, in 1969. He received the Dipl.-Ing. degree from the University of Erlangen-Nürnberg, Germany, in 1996. He is currently working toward the Ph.D. degree at the Laboratories for High Frequency Technology in Erlangen.

He is currently involved in a research project on a new multielement circuit technology for THz frequencies, which is supported by the German Research Council (DFG). His main research interests are the development of passive components for quasi-optical circuits at THz frequencies as well as the development of complex field measurement systems in this frequency region.

Carsten Winnewisser was born in Durham, NC. He received the degree in medical physics and techniques from the University of Kaiserslautern, Germany, in 1997 and the Ph.D. degree in physics from the University of Freiburg, Germany, in 1999.

From 1995 to 1999, he has been working on the generation, detection, and application of THz pulses in the Department of Molecular and Optical Physics, University of Freiburg. Presently he is working as a post-doctoral fellow at the Freiburg Materials Research Center of the University of Freiburg. His interests lie in luminescence conversion with LEDs and in the application of photonic structures in the far infrared and optical region.

Dr. Winnewisser is a fellow of the German Physical Society (DPG).